

TEMPORAL AND SPATIAL HETEROGENEITY IN PULMONARY PERFUSION: A MATHEMATICAL MODEL TO PREDICT INTERACTIONS BETWEEN MACRO- AND MICRO-VESSELS IN HEALTH AND DISEASE

A. R. CLARK^{✉1} and M. H. TAWHAI¹

(Received 4 July, 2017; accepted 22 March, 2018; first published online 7 June 2018)

Abstract

Heterogeneity in pulmonary microvascular blood flow (perfusion) provides an early indicator of lung disease or disease susceptibility. However, most computational models of the pulmonary vasculature neglect structural heterogeneities, and are thus not accurate predictors of lung function in disease that is not diffuse (spread evenly through the lung). Models that do incorporate structural heterogeneity have either neglected the temporal dynamics of blood flow, or the structure of the smallest blood vessels. Larger than normal oscillations in pulmonary capillary calibre, high oscillatory stress contribute to disease progression. Hence, a model that captures both spatial and temporal heterogeneity in pulmonary perfusion could provide new insights into the early stages of pulmonary vascular disease. Here, we present a model of the pulmonary vasculature, which captures both flow dynamics, and the anatomic structure of the pulmonary blood vessels from the right to left heart including the micro-vasculature. The model is compared to experimental data in normal lungs. We confirm that spatial heterogeneity in pulmonary perfusion is time-dependent, and predict key features of pulmonary hypertensive disease using a simple implementation of increased vascular stiffness.

2010 *Mathematics subject classification*: primary 92C35; secondary 92B05, 92C30.

Keywords and phrases: lung, perfusion, mathematical model.

1. Introduction

In order to effectively contribute to gas exchange, the lung's vasculature delivers blood to approximately 130 m^2 of the alveolar surface without putting excessive strain on the heart. The vascular structures in the lung are therefore structurally and functionally different from their systemic equivalents, and form a relatively "low resistance" system. Multiple mechanisms determine the timing and delivery of

¹Auckland Bioengineering Institute, University of Auckland, New Zealand;
e-mail: alys.clark@auckland.ac.nz, m.tawhai@auckland.ac.nz.

© Australian Mathematical Society 2018

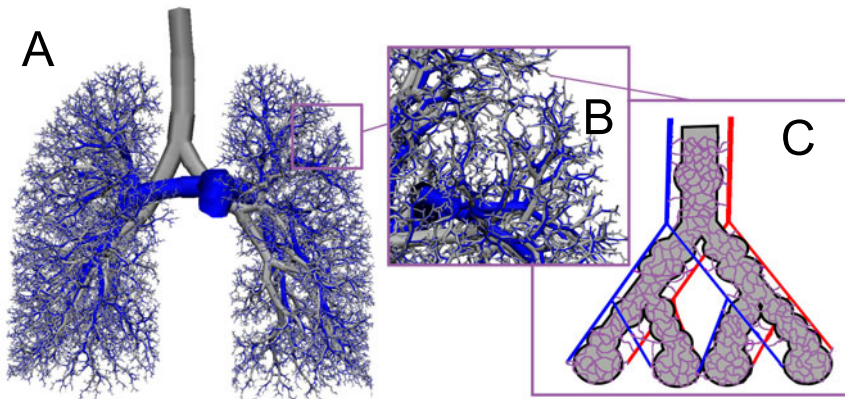


FIGURE 1. Relationship between the structure of pulmonary blood vessels and airways using the model employed in this study for the vasculature. (a) Airways (grey) and arteries (blue) are shown. Each major airway is accompanied by an artery and a vein (not shown). (b) Arteries accompanying airways to the level of the acinus are shown. (c) Schematic of the acinus, consisting of approximately nine generations of small arterioles which give rise to a capillary network (purple) covering the alveolar surface and feeding oxygen rich blood to the pulmonary venules (red) that drain the acinus (colour available online).

blood to the alveolar capillaries (perfusion), including influences from asymmetric vascular branching and gravity. In a normal lung, perfusion is well-matched with alveolar air flow (ventilation) allowing efficient gas exchange. However, knowledge regarding the relative contribution of mechanisms such as gravity and structure to the distribution of perfusion in the lungs is still incomplete [21, 44]. It is clear that heterogeneity in perfusion distribution is significant, and that changes in perfusion heterogeneity seen in functional imaging may be an early indicator of lung disease or disease susceptibility [1, 26, 33], but the mechanisms driving early disease changes (for example, vasoconstriction in the smallest pulmonary vessels versus alveolar destruction) are unclear.

To ensure a large capillary surface area, the pulmonary blood vessels (Figure 1) branch dichotomously over approximately 23 generations to feed approximately 32 000 functional gas exchange units (the acini). Within each acinus, there are multiple generations of extra-capillary arterioles and venules, which feed “sheets” of capillaries covering the alveolar surface. These capillaries are described as filling the space between two thin sheets of alveolar tissue, supported by a capillary diameter apart by posts of tissue, which can be visualized in resin casts of the lung (as presented by Fung and Sobin [16] as part of their detailed theoretical analysis). A “distributed” acinar circulation with serial and parallel connections between arterioles and venules may enable the lung to cope with localized disruption to vascular function without significant increases in blood pressure [8, 11]. The pulmonary circulatory system is embedded in a highly deformable tissue and its deformation has been described as like that of a Slinky™; lung tissue is relatively more compressed in the base of the lung (with respect to gravitational direction) than the apex [27]. Deformation of lung

tissue results in a gradient in pleural pressure over the gravitational height of the lung, causing local variation in alveolar expansion and influencing the calibre and surface areas of capillary beds. The blood pressures internal to the vessel, and elastic recoil due to lung tissue mechanics, oscillate over a heart beat (or a breath); and because the vasculature is compliant, these dynamic changes contribute to delivery of blood to the alveolar tissue. The multiple biophysical factors contributing to blood flow dynamics in the lung, and the differences in the physics of blood flow across multiple scales, means that experimentally interpreting or measuring the contributors to pulmonary blood flow are challenging.

Several mathematical models describing pulmonary blood flow have been proposed. Steady-state models that incorporate the anatomic structure of the pulmonary vasculature, and the key physics of flow across spatial scales have helped to tease apart the major contributors to pulmonary perfusion distribution [3, 4, 10]. Dynamic models of the pulmonary vasculature only consider pulmonary arteries (anatomically structured models) [37, 39], or simplify the pulmonary vascular tree, by approximating vascular structures as symmetric or quasi-symmetric [40, 53, 54]. However, the functions of the lung at small and large scales impact on one another in pulmonary vascular disease [9, 46], thus including both structure and temporal dynamics in a model is important. Here we present a computational model of the dynamic pulmonary vasculature using realistic anatomic representations of the whole circulation to improve the relevance of models of this class to disease. This model is able to predict both spatial and temporal heterogeneity in pulmonary blood flow, consistent with known properties of the distribution of pulmonary perfusion, and provides a framework for modelling the impact of pulmonary hypertensive conditions on whole lung function.

2. Methods

2.1. Model geometry

2.1.1 Subject imaging. A vascular geometry covering the pulmonary arteries and veins was generated from computed tomography (CT) imaging of the lungs of a 23-year-old caucasian nonsmoking male from a human lung atlas database [24, 25]. CT imaging was acquired at controlled lung volumes approximating functional residual capacity (FRC). Imaging of all subjects in the database was approved by the University of Iowa Institutional Review Board and Radiation Safety Committees. The subject was 1.87 m tall, with a weight of 80.9 kg (body mass index 23.1 kg m^{-2}). In the upright posture the subject had lung volumes of 3.40 l, and 7.13 l at FRC and TLC (total lung capacity), respectively. This subject was closest (by Mahalanobis distance) to the mean lung shape in principal component analysis of 30 normal subjects from the human lung atlas database aged between 20 and 30 years.

2.1.2 Large blood vessels. The largest blood vessels were segmented from CT images in the chosen subject to a defined anatomical location (the first generation beyond the segmental arteries). The lobar shapes were also segmented from imaging,

and blood vessels to the level of the acinus were generated to fill this volume and to match morphometric branching properties of the pulmonary vasculature. The generation of vascular geometries from imaging is described in detail by Burrowes et al. [3]. Each (extra-acinar) blood vessel is defined by two nodes connected by an one-dimensional (1D) finite element, representing the vessel centreline, and a constant unstrained radius r_0 (radius at zero transmural pressure, p_{tm}). The arterial geometry for this subject (Figure 1(a)) terminates at 30 676 arteries (and veins) that feed idealized representations of the acinar blood vessels.

2.1.3 Acinar blood vessels. The structure of the acinar blood vessels is modelled as described by Clark et al. [8]. Nine symmetric generations of arterioles and venules are connected at their midpoints by capillary “sheets”, as described from detailed measurements and theoretical analyses by Fung and Sobin [16]. Importantly, the intra-acinar vessels form a “ladder-like” structure with serial and parallel connections to the capillary beds of the lung, representative of the anatomic structure of the lung at this level and neglected from prior dynamic models of the pulmonary circulation.

The complete geometric model comprises 122 720 individual asymmetric vessel elements (arteries and veins), plus explicit representations of nine generations of symmetric arterioles and venules connected by capillary beds at each of 30 676 acinar units. To simulate flow dynamics in the time domain in each of these blood vessels is impractical, and thus we take advantage of wave transmission theory, following a similar approach to simplified geometric models of the pulmonary vasculature [37, 54]. To illustrate the impact of neglecting vascular asymmetry, a symmetric branching structure comparable to the anatomic geometry with 15 branching orders, resulting in $2^{15} = 32\,768$ acinar units was also generated. This model has the closest possible number of vessels as the anatomical model and the same arterial and venous diameters and length at each order [3].

2.2. Elastic properties of arteries, veins and capillaries The relationship between blood vessel radius, r , and transmural pressure, p_{tm} , depends on location in the lung. The difference between blood pressure, p_b , and tethering pressure acting radially on the blood vessel, is denoted as p_{tm} . Tethering pressure is the pleural pressure, p_{pl} , the negative pressure generated in lung tissue as the respiratory muscles pull the lung volume open, if vessel radius is greater than 200 μm and alveolar pressure, p_A , if vessel radius is less than 200 μm [52]. In the extra-acinar blood vessels a linear relationship between r and p_{tm} holds [31]. That is,

$$r = r_0 \left(1 + \frac{3r_0}{4Eh_0} p_{tm} \right) = r_0 (1 + \alpha p_{tm}),$$

where r_0 is the unstrained radius of the artery or vein, E is the elastic modulus of the vessel wall, and h_0 is the thickness of the vessel wall. In the lung macro-vasculature $\alpha = 3r_0/4Eh_0$ is independent of species and vessel size, with $\alpha = 1.49 \times 10^{-4} \text{ Pa}^{-1}$ (0.02 mm Hg $^{-1}$) [31].

The calibre of vessels in the capillary sheet are represented as sheet height, H , which has been shown to be well-represented as a linear function of p_{tm} except when p_{tm} is negative, which is unlikely in a normally breathing lung. Thus,

$$H = H_0 + \alpha_c p_{tm},$$

where α_c is a compliance constant [18], and H_0 is the unstrained sheet height.

2.3. Wave transmission: admittance of model elements

2.3.1 Extra-capillary blood vessels. Wave transmission in the large (extra-acinar) arteries and veins and the intra-acinar arterioles and venules is modelled following [12], which applies a viscous correction term to classical inviscid models [15, 51]. Arteries and veins are assumed to be thin walled elastic tubes, flow within them is axisymmetric, laminar and fully developed following a Womersley velocity profile [12, 13, 50]. The model also assumes that the wavelength of transmitted and reflected waves is much greater than vessel radius throughout the lung. Under these assumptions, the Navier–Stokes equations reduce to the wave equation, whose solutions provide a description of pressure and flow as a superposition of an incident and reflected wave in each vessel. Each arterial and venous segment in the pulmonary circulation is then defined by a characteristic wave velocity, c_c , and a characteristic admittance Y_c as

$$c_c^2 = \frac{2Eh_0}{3r_0\rho} \epsilon_r = \frac{\epsilon_r}{2\alpha\rho}, \quad Y_c = \frac{\pi r_0^2}{\rho c_0} \sqrt{\epsilon_r},$$

where ρ is blood density, and ϵ_r provides the viscous correction

$$\epsilon_r = 1 - F_{10}(W), \quad F_{10}(W) = \frac{2J_1(i^{3/2}W)}{Wi^{3/2}J_0(i^{3/2}W)}$$

with J_0 and J_1 Bessel's functions of order 0 and 1, respectively, $i = \sqrt{-1}$, and $W = r_0 \sqrt{\omega\rho/\mu}$ is the Womersley number for the vessel in question, with ω defined as harmonic frequency and μ as blood viscosity. The wave propagation constant associated with these vessels is defined as $\gamma = i\omega/c_c$.

2.3.2 Capillary sheet admittance. Characteristic admittance of the capillary sheet is derived from the theoretical considerations of [14]. This model assumes that capillary beds can be well-approximated as a “sheet” of blood vessels separated by “posts” of tissue with much smaller sheet height than width or length (capillary diameter is small compared with the size of an alveolus or acinus). A low Reynolds number flow is assumed, and in the steady-state an analytical relationship between volumetric flow and capillary transmural pressure can be derived [10, 18]. In the time-dependent problem, if one assumes small oscillations in blood pressure at the capillary level and fluid loss due to the permeability of alveolar walls is negligible, the governing equations can be linearized and a concept of admittance becomes relevant [18]. Admittance is described by two second order ordinary differential equations (per capillary sheet). If one makes the further assumption that sheet height is almost

constant along its length, which is reasonable at the level of a single alveolus, then characteristic input admittance for the sheet is

$$Y_c = \sqrt{\frac{\omega L_c^2 H^3 \alpha_c i}{\mu F k}},$$

where ω is harmonic frequency, L_c is the average pathlength through the sheet from arteriole to venule, and F and k are numerical constants comprising a “friction factor” (note that this admittance is given in physical units derived from the nondimensional analysis of [14]). The corresponding wave propagation constant $\gamma = \sqrt{i\mu_c F k \omega \alpha_c / H^3}$.

2.4. Network wave transmission

2.4.1 *Effective admittance.* Effective admittance Y_e is calculated for each vessel segment by considering reflections of waves at bifurcations. This Y_e is used to calculate pressure and flow waveforms through the whole system and is defined as

$$Y_e = Y_c \frac{(1 - R e^{-2\gamma L})}{(1 + R e^{-2\gamma L})},$$

where L is vessel length (or capillary path length), and R is a reflection coefficient which determines the level of wave reflection back into the blood vessel at a bifurcation. Multiple wave reflections are not considered, as in previous pulmonary wave transmission models [19, 53].

2.4.2 *Wave reflections in arteries (diverging tree).* In the arterial tree, each parent branch bifurcates to two daughter branches. The wave reflection coefficient, R , at the bifurcation is a function of the admittances of the parent vessel and the two daughter vessels [29],

$$R = \frac{Y_c^p - Y_e^{d1} - Y_e^{d2}}{Y_c^p + Y_e^{d1} + Y_e^{d2}};$$

here superscripts p denote the parent and $d1$ and $d2$ denote daughter vessels.

2.4.3 *Wave reflections in arteries (converging tree).* At each venous bifurcation two sister branches, $S1$ and $S2$, converge on a single daughter, d . Duan and Zamir [13] derived the reflection coefficient in each of $S1$ and $S2$ as

$$R^{S1} = \frac{Y_c^{S1} + (2H - 1)Y_c^{S2} - Y_e^d}{Y_c^{S1} + Y_c^{S2} + Y_e^d}, \quad R^{S2} = \frac{(2/H - 1)Y_c^{S1} + Y_c^{S2} - Y_e^d}{Y_c^{S1} + Y_c^{S2} + Y_e^d},$$

where

$$H = \frac{\bar{p}^{S2} e^{-\gamma^{S2} L^{S2}}}{\bar{p}^{S1} e^{-\gamma^{S1} L^{S1}}},$$

with \bar{p}^j the pressure amplitude, γ^j the wave propagation constant, and L^j the length of vessel $j = S1, S2$. In a symmetric system, $S1 = S2$ and $H = 1$.

2.5. Pressure and flow profiles through the vascular tree Defining the incident transmural pressure waveform at the inlet of the vessel which extends from $x = 0$ to $x = L$ to be $p_0 e^{i\omega t}$,

$$p(x, t) = p_0 e^{i\omega t - \gamma x} + p_0 R e^{i\omega t + \gamma x - 2\gamma L},$$

and flow $q(x, t)$ along the length of a vessel is

$$q(x, t) = p_0 Y_c e^{i\omega t - \gamma x} - p_0 Y_c R e^{i\omega t + \gamma x - 2\gamma L}. \quad (2.1)$$

Once effective admittances and reflection coefficients have been calculated for the entire vascular system, given a defined value of p_0 in the inlet artery (the main pulmonary artery), one can step through the tree and calculate p_0 for each vessel in the system using

$$p_{0d} = p_{0u} \frac{(1 + R_u) e^{-\gamma_u L_u}}{1 + R_d e^{-2\gamma_d L_d}},$$

where subscripts u and d represent upstream and downstream vessels, respectively. The flow profile in each vessel can then be derived from the pressure profile using equation (2.1).

2.6. Gravity and boundary conditions Gravity is incorporated into the model via a linear increase in pleural pressure, p_{pl} , down the lung acting externally to the vasculature, from a mean value of -490.3 Pa (-5 cm H₂O). p_{pl} is then variable in space, but constant in time. In the governing equations, it is p_{tm} that is the relevant pressure, but note that p_{tm} depends on p_{pl} at the macro- but not micro-scale, thus the impact of p_{pl} on macro-scale p_b impacts on the micro-scale p_{tm} . This gradient has been estimated experimentally to be 24.52 Pa cm⁻¹ lung height (0.25 cm H₂O cm⁻¹) [47]. The steady component of the model approaches the steady model used in our previous studies of the pulmonary vasculature [10]. In addition, a constant body force term acting along the major axis of the vessel is applied: $g_x = \rho g \cos \theta$, where ρ is blood density, g is gravitational acceleration, and θ is the angle the vessel makes with the vertical axis (the direction of gravity). It should be noted that to simplify the model no capillary collapse or recruitment is incorporated beyond their impact on capillary sheet height. In terms of West's classic zonal descriptions of lung perfusion [48], capillary collapse occurs if there is high alveolar pressure relative to blood pressure, however, this is not a feature of the steady model under normal conditions [10], and thus is unlikely to impact on results presented here as alveolar pressure is fixed at zero (atmospheric pressures) and negative blood pressures are not predicted.

A pressure waveform is applied at the inlet to the model, the main pulmonary artery. The waveform is derived from a typical pulmonary artery pressure waveform [5], and assumed to take the form

$$p_0(t) = A_0 + \sum_{n=1}^{n=N} A_n \cos(\omega t + \phi_n), \quad (2.2)$$

where ω is harmonic frequency ($\omega = 2\pi n HR/60$, with HR representing heart rate), A_n and ϕ_n are least-squares fits to the pressure waveform, given in Table 1. For an outlet boundary condition, we assume wave reflection at the left atrium (exit of the veins)

TABLE 1. Definition of the parameters A_n (Pascals) and ϕ_n (radians) from equation (2.2) that characterize the pressure waveform at the inlet of the model (the main pulmonary artery).

n	0	1	2	3	4	5	6	7	8	9	10
A_n	2038	846	325	188	-82.6	-47.6	-65.4	41.6	13.9	-30.4	22.2
ϕ_n	-	4.37	3.64	3.18	5.11	2.31	0.63	2.51	5.95	0.81	2.73

TABLE 2. Definition of model parameters representing a healthy pulmonary vasculature.

Parameter	Description	Value	Source
<i>Structural parameters (subject specific)</i>			
r_0 (MPA)	Main pulmonary artery unstrained radius	12.0 mm	[10]
R_d (artery)	Strahler diameter ratio (arteries)	1.54	[10]
r_0 (MPV)	Main pulmonary venous unstrained radius	14.8 mm	[10]
R_d (vein)	Strahler diameter ratio (veins)	1.55	[10]
<i>Extra-acinar parameters</i>			
α	Vessel compliance	$1.49 \times 10^{-4} \text{ Pa}^{-1}$	[31]
μ	Blood viscosity	$3.36 \times 10^{-3} \text{ Pa s}$	[38]
ρ	Blood density	$1.05 \times 10^{-6} \text{ kg mm}^{-3}$	[38]
<i>Intra-acinar parameters</i>			
α_c	Capillary sheet compliance	$1.3 \times 10^{-9} \text{ m Pa}^{-1}$	[15]
F	Friction factor constant	1.8	[17]
k	Friction factor constant	12.0	[17]
H_0	Unstrained capillary height	$3.5 \times 10^{-6} \text{ m}$	[15]
L_c	Average pathlength from arteriole to venule	$1186 \times 10^{-6} \text{ m}$	[53]
μ_c	Apparent blood viscosity in capillaries	$1.92 \times 10^{-3} \text{ Pa s}$	[15]

is negligible. An impedance boundary condition at the left atrium was also considered, based on measurements from [35], but this boundary condition did not impact on the model results presented here. A typical heart rate of 75 beats per minute is assumed.

2.7. Model parameterization and implementation The model is parameterized to represent a normal, healthy lung vasculature. Parameters are chosen exactly as described by Clark et al. [10] in their steady model of perfusion and are given in Table 2. The model is implemented in a custom written Fortran library based on the CMISS infrastructure (www.cmiss.org). The full model takes 5–6 min to run on a desktop computer with 16GB RAM and a 3.4 GHz processor (including

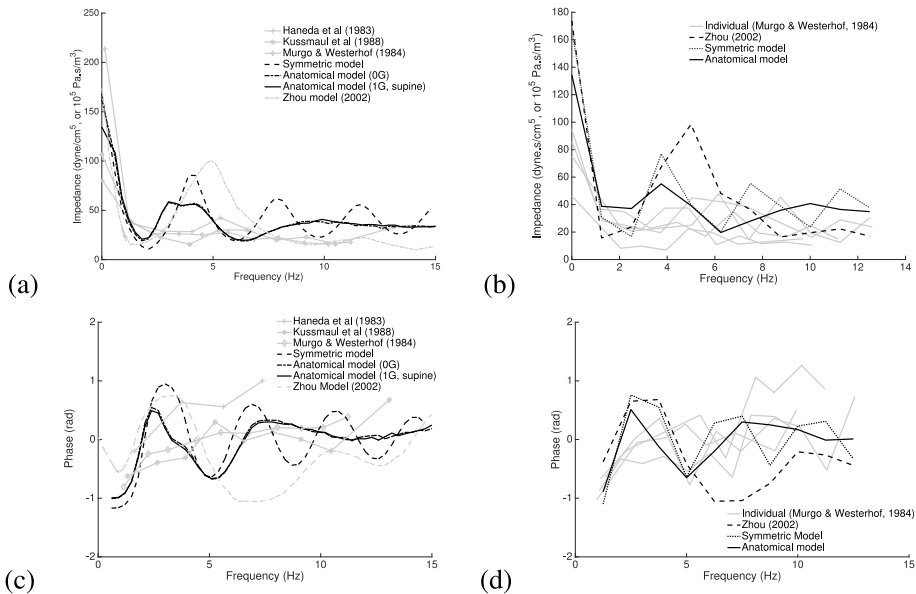


FIGURE 2. (a), (b) Impedance magnitude and (c), (d) phase spectra for the main pulmonary artery as measured experimentally [22, 32, 34] and as predicted by our model in a symmetric geometry, and an anatomically based geometry (with and without gravity) as well as a previous model of the human pulmonary circulation [53]. In (a), (c) model predicted spectra are shown as continuous, as is the convention in modelling studies, and experimental data are averaged in both frequency and impedance/phase. In (b), (d) model results are presented in the same manner as experimental data in individuals and five individual datasets from [34] are shown for comparison.

geometrical set up). Simulations are conducted supine, as this is the most prevalent posture for imaging, and the likely posture in impedance studies, which require heart catheterization.

3. Results

3.1. The normal lung Pulmonary artery impedance (the reciprocal of admittance) spectra provide a clinically measurable model output for comparison to model predictions. This measure reflects the combined effects of compliance and wave reflection through the system, and is proposed as a key measure of vascular dysfunction [6, 28]. Impedance spectra measured in cohorts of normal humans are typically averaged by the frequency of each harmonic of the heart beat and by the value of impedance at each harmonic [22, 32, 34]. These are compared to model predictions using: (1) the symmetric geometry, (2) the anatomical model with no gravitational effects and (3) the full model as shown in Figure 2. The full model shows better agreement with measured data than the symmetric model or a previous quasi-symmetric model [53]. Impedance spectra between individuals are highly variable (Figure 2(b) or (d)) but typically present with a high zero frequency impedance,

TABLE 3. Impedance spectra as predicted by the model at the acinar level, the mean impedance magnitude (Z), coefficient of variation (COV) and gradient over gravitational height (g) for the first two harmonics are shown here. Impedance is given in typical respiratory physiology units dyne s cm^{-5} which is equivalent to 10^5 Pa s m^{-3} .

	First harmonic			Second harmonic		
	$Z \times 10^5$ (dyne s cm^{-5})	COV (%)	$g \times 10^5$ (dyne s cm^{-6})	$Z \times 10^5$ (dyne s cm^{-5})	COV (%)	$g \times 10^5$ (dyne s cm^{-6})
Symmetric	153.0	0	0	114.3	0	0
Anatomic (0G)	107.7	66.44	0.21	78.9	43.39	0.08
Anatomic (1G)	124.3	60.37	3.57	89.98	42.64	2.15

followed by a minimum at 1–3.5 Hz [36] (1.8 Hz in the model), followed by one or more minima, and asymptote to the characteristic impedance of the system, 22–40 dyne s cm^{-5} in normal humans [22, 32, 34] (33 dyne s cm^{-5} in the model). Symmetric and quasi-symmetric models overestimate the height of the first peak in the impedance spectrum compared to the anatomic model. The symmetric model predicts several regularly spaced local maxima of the impedance spectrum. In comparison, asymmetry in branching in the anatomically based model results in wave reflection and thus fewer distinct maxima are visible. The effect of gravity on input impedance spectra is small as main pulmonary artery impedance spectra predominantly reflect the function of the proximal pulmonary arteries, whereas gravitational effects are more distinct distally. Phase spectra show a tendency for increasing phase with frequency with some oscillation, which is in general captured by both anatomic and symmetric models. However, the considerable variation between individuals in phase makes interpretation of which model best captures phase spectra difficult. The phase spectrum predicted by a previous quasi-symmetric model [53] does however sit below expected phase spectra at high frequencies and thus our model provides improvement in this regard.

Impedance spectra are also calculated at the acinar level (the first acinar arteriole), and show a progressively decreasing magnitude of impedance with frequency, consistent with a previous model of dog lungs [19]. Table 3 shows acinar impedance magnitude for the first two harmonic frequencies, and quantifies the coefficient of variation and gradient (in the gravitational axis) of impedance in each model solved. The symmetric model predicts all impedances to be equal, as each acinus has the same upstream/downstream impedance, when anatomic structure is added variation is seen in acinar impedance. Finally, the effects of gravity are to introduce a gradient in acinar impedance with increased impedance at the gravitationally nondependent (anterior) regions of the lung. Figures 3 and 4 show the spatial distribution of pulmonary perfusion predicted over the course of a heart beat. Perfusion is nonuniform over lung height with a relatively higher blood flow rate in gravitationally dependent (posterior) regions of the lung than in the nondependent (anterior) regions of the lung. There is

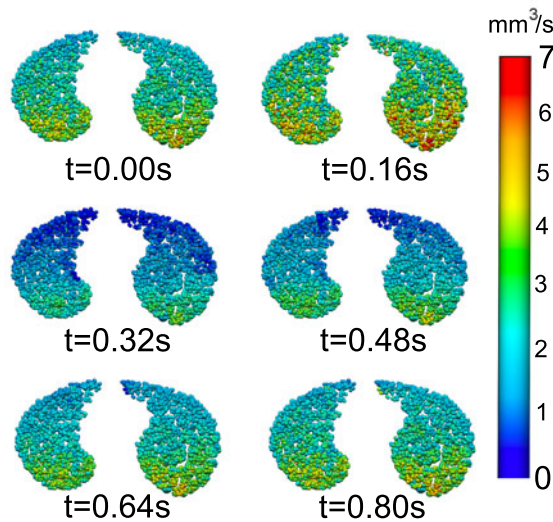


FIGURE 3. Predicted spatial distribution of pulmonary perfusion over a heart beat, in a slice through the supine lung. Results are shown at the level of the arterioles feeding the acinus. There is a gravitational distribution in perfusion through the heart beat, with higher blood flow rate in the gravitationally dependent (posterior) regions of the lung than the nondependent (anterior) regions (colour is available online).

a relatively higher amplitude of flow waves predicted in the gravitationally dependent regions of the lung (but a relatively lower mean flow). In Figure 4, blood flow rates are binned in 10 mm slices over the height of the lung, typical of magnetic resonance slice thickness [27], to illustrate gravitational gradients and heterogeneity in perfusion. Again, the anatomical structure can be seen to lead to heterogeneity in flow, and gravity adds a gradient to this flow. The model predicts that both the gravitational gradient in blood flow and heterogeneity is temporally variable. In addition, due to varying pathlengths from right to left heart, the model predicts some “clustering” of acinar units with similar flow patterns which are relatively independent of gravitational location. These clusters typically contain 7–20 acinar units, and appear to have relatively higher, or lower pathlengths to the main pulmonary trunk than is typical for their gravitational location within the lung.

3.2. The impact of arterial stiffening Arterial stiffening typically occurs in pulmonary hypertension [43]. The consequence of arterial stiffening is hypothesized to be an increase in pressure wave pulse propagation to the distal vasculature, leading to inflammation and injury in the distal pulmonary vasculature [43]. To assess model behaviour under pulmonary arterial stiffening, we decreased the parameter α representing compliance of the large arterial tree to 50% and 25% of its baseline values, consistent with expected changes in compliance due to vascular wall thickening [23]. The decrease in α was applied uniformly throughout the model geometry in

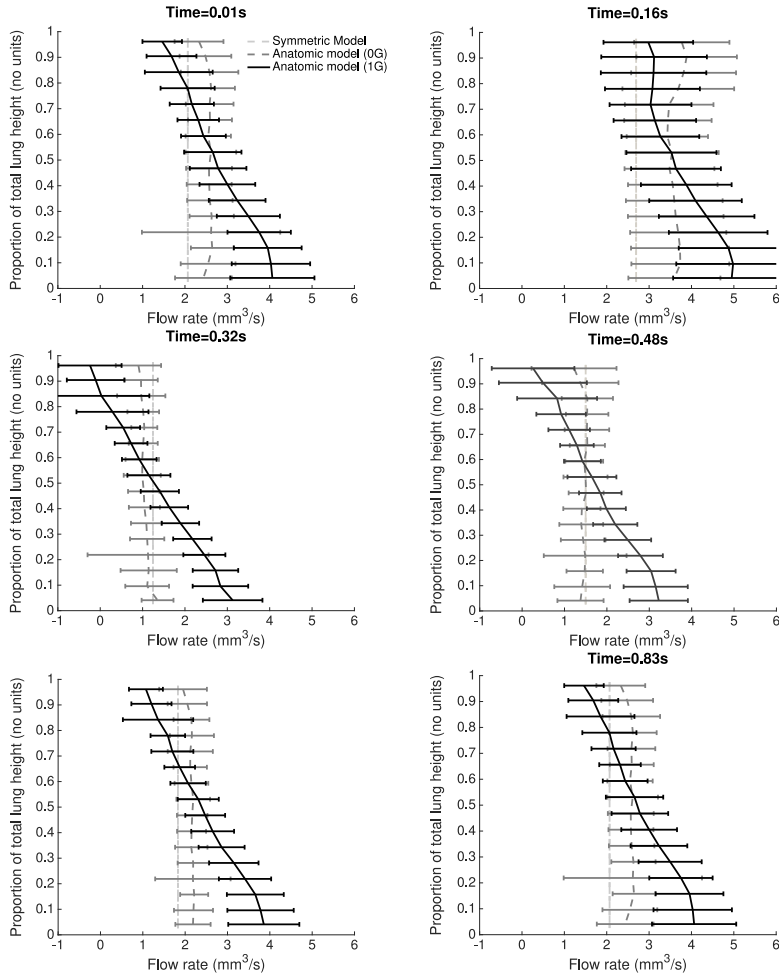


FIGURE 4. Predicted pulmonary perfusion distribution over a heart beat, averaged in 10 mm bins over the height of the lung in symmetric, zero gravity and full anatomic models. There is variation in the gravitational gradient, and heterogeneity, of blood flow over the heart beat, with gravitationally nondependent (anterior) regions having a relatively greater amplitude of blood flow variation than dependent (posterior) regions. Simulations are conducted supine with anterior edge of the lung at height 1, and the posterior edge at height 0.

extra-acinar vessels. Decreasing α in general increases flow velocity pulse amplitude, with the median per acinus ratio of velocity amplitude in the arterioles to baseline values being 1.94. Despite homogeneous changes in α this impact is variable through the lung. Figure 5 shows the redistribution of flow over a heart beat for decreasing α . The asymmetric structure of the vasculature results in a nonhomogeneous reduction in vascular diameter, and thus some over- and under-perfused regions of the lung. Small clusters of either high or low amplitude flow waveforms, due to (relatively) high and

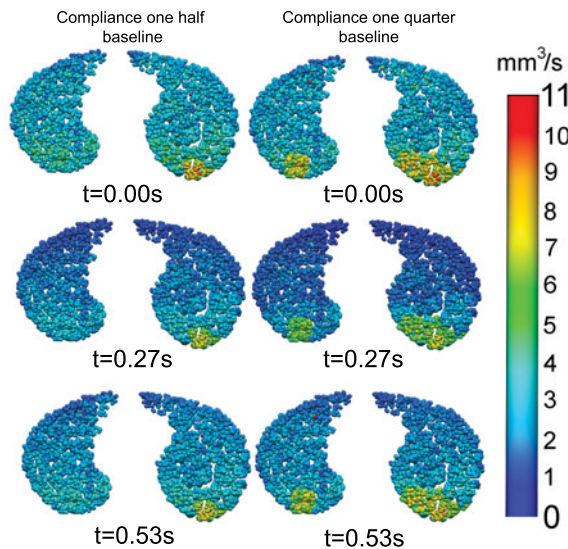


FIGURE 5. Predicted spatial distribution of pulmonary perfusion over a heart beat, in a slice through the supine lung at the level of the arterioles feeding the acinus. Model predictions are shown for cases of vascular stiffening, which is a feature of pulmonary hypertension. The parameter defining large vessel compliance, α is reduced to 50% and 25% of its baseline value. Regional “patchiness” in perfusion distribution is observed, and a small shift toward higher amplitude flow oscillation (colour available online).

low resistance pathways that were present in baseline simulations, emerge as larger clusters. This is similar to the impact of airway constriction in anatomical models of the lung, where constriction of an already small pathway has a greater impact than on relatively larger pathways [45]. This pattern may be reflective of “mosaic” patterns in CT images of patients with primary pulmonary arterial hypertension [30]. Model predictions of main pulmonary artery input impedance are consistent with observations in pulmonary vascular disease [6], with increasing zero frequency impedance (increasing admittance) of $134.4 \text{ dyne cm}^{-5}$ at baseline, $161.3 \text{ dyne cm}^{-5}$ with α at 50% of baseline, and $198.8 \text{ dyne cm}^{-5}$ with α at 25% of baseline. The model also predicts an increase in the frequency of the first minimum of the impedance spectrum ($1.8, 2.7, 3.6 \text{ Hz}$ at baseline, 50% and 25% values of α , respectively), also consistent with spectra observed in pulmonary vascular disease [6].

4. Discussion

In this study, we present a model of pulse wave transmission in the pulmonary circulation, that captures key contributors to blood flow distribution, and is simple enough to solve within an anatomical model of the whole pulmonary vasculature. The model improves upon existing models of the pulmonary circulation that assume idealized representations of vascular structure [40, 53, 54] and that consider the arterial

tree in isolation [37, 39], or are steady-state [3, 4, 10]. Incorporating the dynamics of blood flow is essential in predicting the impact of pulmonary vascular disease, as pulmonary vascular resistance or mean blood pressure are not always reflective of disease severity, rather it is the impedance of the system or the relationship between pulse pressures and flow that determines the strain on the right heart [28].

The incorporation of an anatomically based acinar structure is a unique advantage of this model, as it allows predictions of whole lung function when small vascular structures are altered. It also allows prediction of small scale vascular function in response to proximal pulmonary artery stiffening or obstruction. A major question regarding pulmonary hypertension, is the extent to which vascular stiffening in the largest and smallest pulmonary arteries impacts on subsequent shear stress mediated vascular remodelling [43]. We have previously demonstrated that small arterial remodelling results in a propagation of increasing wall shear stress through the arterial tree [37], and here we confirm that large arterial stiffening modulates flow pulse propagation to the small arterioles, largely increasing oscillations in flow (and so shear stress) but with regional heterogeneity. Heterogeneity in perfusion distribution is a significant contributor to disease, and future applications of this model may enable distinction between different classes of pulmonary vascular disease by relating characteristic changes in the micro-vasculature to clinically measurable quantities such as impedance spectra. For example, heterogeneity in pulmonary perfusion in emphysema susceptible smokers [1] has been proposed to be due to hypoxic pulmonary vasoconstriction in the small arterioles, but may also be due to micro-emphysema (undetectable with current *in vivo* imaging technologies). This class of model, along with models of ventilation [42] and hypoxic vasoconstriction [2], may provide a means to distinguish between the two potential mechanisms.

An important clinical measurement to assess severity of pulmonary vascular disease is the impedance and phase spectra of the main pulmonary artery. Acknowledging patient-specific variation in these spectra [22, 32, 34], our model predicts impedance and phase spectra at least as well as existing models of the system that simplify anatomical structure and predict a single value of acinar impedance for the whole lung [53]. Our model shows quantitative agreement with descriptions of the first minimum and asymptote of the impedance spectrum [36], and improves on previous models in predicting the magnitude of the first peak in the spectrum and the phase. The model also shows qualitative agreement to the response of impedance spectra to vascular stiffening [6]. It shows that the impact of arterial asymmetry on main pulmonary artery impedance spectra is to increase wave reflection, damping the contribution of high frequency oscillations to the impedance spectra. Increasing vascular stiffness increases overall impedance and increases the frequency of the first minimum of the impedance spectrum.

Our model predicts perfusion distribution to be determined by both vascular structure and gravity with a distribution consistent with a previous steady model and imaging data [10]. The contributors to flow distribution and the amplitude of oscillations in blood flow locally are in places competing. In the gravitationally

nondependent regions of the lung (anterior regions when supine) there is a relatively higher pleural pressure which “pulls” on the vasculature, enabling expansion of the larger vessels. However, hydro-static pressure and the balance of blood and air pressure determines capillary level patency (West’s zones of flow [48]) and also contribute to flow dynamics. In general, our model predicts a lower mean flow, and higher amplitude of pulsatile flow in the gravitationally dependent lung, which is consistent with studies suggesting increased temporal heterogeneity in “low flow” regions of the lung [20]. Acinar units with similar flow amplitudes and dominant frequencies are spatially clustered, and this is not simply a function of gravity, which is consistent with experiment [20]. This spatial clustering increases when differences in resistance of arterial pathways are amplified (vessel stiffening), suggesting an important role of downstream and upstream vasculature in driving local flow dynamics. The model predicts nonuniform clustering of disease, typical of pulmonary vascular disease, despite uniform changes in vessel compliance. Nonuniform disease presentation would amplify the clustering of high and low perfusion areas and regions of over and under perfusion in images could potentially be used to infer regional disease progression using a model of this type.

The model is limited to the assumptions made in deriving wave transmission theory, that is, the governing equations for flow through the system can be appropriately linearized. Several key assumptions have been assessed in detail in mammals, where wave transmission theory has been applied to model pulmonary vascular function in simplified geometrical models [49]. That the pulmonary vascular input impedance in an individual is relatively insensitive to heart rate [49] and mode of respiration [34], suggests that the system as a whole behaves approximately linearly. We tested the assumption that wavelengths are small compared with vessel radius by calculating wavelength through the vascular tree, and our calculated wavelengths were at least ten times higher than radius throughout. Multiple wave reflections were neglected as the rate of change of vessel diameter with order led to predictions of a decrease in reflected wave amplitude with each subsequent reflection. An analysis of the relative amplitude of the first harmonic of reflected to incident waves through the tree suggests that in the symmetric model this ratio is less than 0.2 everywhere and in the anatomic case, it is less than 0.5 everywhere. Thus, the amplitude of the reflected wave can be expected to decrease with each subsequent reflection. However, inclusion of multiple reflections may be a useful improvement to the model in the future.

Pressure harmonics have been shown to attenuate significantly in the smallest pulmonary arteries and capillaries [34], justifying the assumption of small oscillations at this level [14]. In the capillary portion of the model, we have made the simplifying assumption that capillary sheet height is almost constant along its length, allowing us to employ an analytical description of capillary admittance. This assumption is most correct in gravitationally dependent regions of the lung, as in nondependent regions there is the potential for partial or complete capillary closure [14]. However, previous static models of pulmonary perfusion [10] suggest that this type of capillary closure is not to be expected in normal, negative pressure breathing. This assumption can

be overcome by solving two ordinary differential equations at each of the model's $30\,676 \times 2^9$ capillary beds [14], which will significantly increase solution time. This, however, would increase model applicability and robustness in simulating diseased states. Similarly, we have assumed unstrained radius to be constant along the length of a vessel. This assumption is not well-tested in the biological literature, but may not be the case, particularly near bifurcations. In general, network models such as this underestimate the impact of bifurcation structure on flow, and testing using detailed computational fluid dynamics models of arterial structure across a range of spatial scales may improve assumptions made at this level in future.

Finally, external influences on pulmonary vascular function (alveolar and pleural pressure) are assumed constant in time. In the breathing lung, these pressures are oscillatory with a frequency of approximately 12 breaths per minute compared to a heart rate of approximately 75 beats per minute. An improvement to this model would be to incorporate these oscillations, providing the opportunity to loosely couple to models of ventilation [42], potentially using the methodology described by Chaturani and Isaac [7], or by Sud and Sekhon [41]. This improvement to the model is most likely worthwhile when considering mechanical ventilation strategies when alveolar pressure may become high, as in normal breathing alveolar pressure is close to atmospheric pressure.

In summary, in this study we have presented a model of the dynamics of blood flow in an anatomically structured model of the lung, which can predict flow rates and pressure profiles through the whole pulmonary circulation with boundary conditions only at the heart. This model provides a basis for predicting the impact of pulmonary vascular disease on clinical metrics in models representative of individual patients, which may be used to guide treatment strategies in future.

Acknowledgement

A. R. Clark is supported by the Rutherford Discovery Fellowship (14-UOA-019) of the Royal Society of New Zealand.

References

- [1] S. K. Alford, E. J. R. van Beek, G. McLennan and E. A. Hoffman, "Heterogeneity of pulmonary perfusion as a mechanistic image-based phenotype in emphysema susceptible smokers", *Proc. Natl Acad. Sci.* **107** (2010) 7485–7490; doi:10.1073/pnas.0913880107.
- [2] K. S. Burrowes, A. R. Clark, M. Wilsher, D. Milne and M. H. Tawhai, "Hypoxic pulmonary vasoconstriction as a contributor to response in acute pulmonary embolism", *Ann. Biomed. Eng.* **42** (2014) 1631–1643; doi:10.1007/s10439-014-1011-y.
- [3] K. S. Burrowes, P. J. Hunter and M. H. Tawhai, "Anatomically based finite element models of the human pulmonary arterial and venous trees including supernumerary vessels", *J. Appl. Phys.* **99** (2005) 731–738; doi:10.1152/jappphysiol.01033.2004.
- [4] K. S. Burrowes and M. H. Tawhai, "Coupling of lung tissue tethering force to fluid dynamics in the pulmonary circulation", *Int. J. Numer. Methods Biomed. Eng.* **26** (2010) 862–875; doi:10.1002/cnm.1386.
- [5] A. C. Burton, *Physiology and biophysics of the circulation: An introductory text* (Year Book Medical Publishers, Chicago, IL, 1972).

- [6] H. C. Champion, E. D. Michelakis and P. M. Hassoun, "Comprehensive invasive and noninvasive approach to the right ventricle-pulmonary circulation unit: state of the art and clinical research implications", *Pulm. Vasc. Dis.* (2009) 992–1007; doi:10.1161/CIRCULATIONAHA.106.674028; *Circulation*(120).
- [7] P. Chaturani and A. S. A. Wassf Isaac, "Blood flow with body acceleration forces", *Int. J. Eng. Sci.* **33** (1995) 1807–1820; doi:10.1016/0020-7225(95)00027-U.
- [8] A. R. Clark, K. S. Burrowes and M. H. Tawhai, "Contribution of serial and parallel micro-perfusion to spatial variability in pulmonary inter- and intra-acinar blood flow", *J. Appl. Phys.* **108** (2010) 1116–1126; doi:10.1152/jappphysiol.01177.2009.
- [9] A. R. Clark, D. Milne, M. Wilsher, K. S. Burrowes, M. Bajaj and M. H. Tawhai, "Lack of functional information explains the poor performance of 'clot load scores' at predicting outcome in acute pulmonary embolism", *Respir. Physiol. Neurobiol.* **190** (2014) 1–13; doi:10.1016/j.resp.2013.09.005.
- [10] A. R. Clark, M. H. Tawhai, E. A. Hoffman and K. S. Burrowes, "The interdependent contributions of gravitational and structural features to perfusion distribution in a multiscale model of the pulmonary circulation", *J. Appl. Physiol.* **110** (2011) 943–955; doi:10.1152/jappphysiol.00775.2010.
- [11] R. L. Conhaim, G. S. Segal and K. E. Watson, "Arterio-venous anastomoses in isolated perfused rat lungs", *Phys. Rep.* **4** (2016) e13023; doi:10.14814/phy2.13023.
- [12] B. Duan and M. Zamir, "Viscous damping in one-dimensional wave transmission", *J. Acoust. Soc. Amer.* **92** (1992) 3358–3363; doi:10.1121/1.404185.
- [13] B. Duan and M. Zamir, "Reflection coefficients in pulsatile flow through converging junctions and the pressure through a converging loop", *J. Biomech.* **26** (1993) 1439–1447; doi:10.1016/0021-9290(93)90094-U.
- [14] Y.-C. Fung, "Theoretical pulmonary microvascular impedance", *Ann. Biomed. Eng.* **1** (1972) 221–245; doi:10.1007/BF02584209.
- [15] Y. C. Fung, *Biodynamics: Circulation* (Springer, New York, NY, 1984).
- [16] Y.-C. Fung and S. S. Sobin, "Theory of sheet flow in pulmonary alveoli", *J. Appl. Phys.* **26** (1969) 472–488; doi:10.1152/jappl.1969.26.4.472.
- [17] Y.-C. Fung and S. S. Sobin, "Elasticity of the pulmonary alveolar sheet", *Circ. Res.* **30** (1972) 451–469; doi:10.1161/01.RES.30.4.451.
- [18] Y. C. Fung and S. S. Sobin, "Pulmonary alveolar blood flow", *Circ. Res.* **30** (1972) 470–490; doi:10.1161/01.RES.30.4.470.
- [19] R. Z. Gan and R. T. Yen, "Vascular impedance analysis in dog lung with detailed morphometric and elasticity data", *J. Appl. Phys.* **77** (1994) 706–717; doi:10.1152/jappl.1994.77.2.706.
- [20] R. W. Glenny, N. L. Polissar, S. McKinney and H. T. Robertson, "Temporal heterogeneity of regional pulmonary perfusion is spatially clustered", *J. Appl. Phys.* **79** (1995) 986–1001; doi:10.1152/jappl.1995.79.3.986.
- [21] R. W. Glenny and H. T. Robertson, "Spatial distribution of ventilation and perfusion: mechanisms and regulation", *Compr. Phys.* **1** (2011) 373–395; doi:10.1002/cphy.c100002.
- [22] T. Haneda, T. Nakajima, K. Shirato, S. Onodera and T. Takishima, "Effects of oxygen breathing on pulmonary vascular impedance in patients with pulmonary hypertension", *Chest* **83** (1983) 520–527; doi:10.1378/chest.83.3.520.
- [23] D. Heath and J. E. Edwards, "The pathology of hypertensive pulmonary vascular disease: a description of six grades of structural changes in the pulmonary arteries with special reference to congenital cardiac septal defects", *Circulation* **18** (1958) 533–547; doi:10.1161/01.CIR.18.4.533.
- [24] E. A. Hoffman et al., "Characterization of the interstitial lung diseases via density-based and texture-based analysis of computed tomography images of lung structure and function", *Acad. Rad.* **10** (2003) 1104–1118; doi:10.1016/S1076-6332(03)00330-1.
- [25] E. A. Hoffman et al., "The comprehensive imaging-based analysis of the lung: a forum for team science", *Acad. Radiol.* **11** (2004) 1370–1380; doi:10.1016/j.acra.2004.09.005.

- [26] S. R. Hopkins, J. Garg, D. S. Bolar, J. Balouch and D. L. Levin, "Pulmonary blood flow heterogeneity during hypoxia and high-altitude pulmonary edema", *Am. J. Respir. Crit. Care Med.* **171** (2005) 83–87; doi:10.1164/rccm.200406-707OC.
- [27] S. R. Hopkins, S. C. Henderson, D. L. Levin, K. Yamada, T. Arai, R. B. Buxton and G. K. Prisk, "Vertical gradients in regional lung density and perfusion in the supine human lung: the slinky effect", *J. Appl. Phys.* **103** (2007) 240–248; doi:10.1152/japplphysiol.01289.2006.
- [28] S. Huez, S. Brimiouille, R. Naeije and J.-L. Vachiéry, "Feasibility of routine pulmonary arterial impedance measurements in pulmonary hypertension", *Chest* **125** (2004) 2121–2128; doi:10.1378/chest.125.6.2121.
- [29] G. Karreman, "Some contributions to the mathematical biology of blood circulation. Reflections of pressure waves in the arterial system", *Bull. Math. Biophys.* **14** (1952) 327–350; doi:10.1007/BF02477850.
- [30] S. J. Kligerman, T. Henry, C. T. Lin, T. J. Franks and J. R. Galvin, "Mosaic attenuation: etiology, methods of differentiation and pitfalls", *RadioGraphics* **35** (2015) 1360–1380; doi:10.1148/rg.2015140308.
- [31] G. S. Krenz and C. A. Dawson, "Flow and pressure distributions in vascular networks consisting of distensible vessels", *Am. J. Phys.: Heart Circ. Phys.* **284** (2003) H2192–H2203; doi:10.1152/ajpheart.00762.2002.
- [32] W. G. Kussmaul, J. M. Wieland and W. K. Laskey, "Pressure-flow relations in the pulmonary artery during myocardial ishaemia: implications for right ventricular function in coronary disease", *Cardiovasc. Res.* **22** (1988) 627–638; doi:10.1093/cvr/22.9.627.
- [33] M. F. Vidal Melo, T. Winkler, R. S. T. Harris, G. Musch, R. E. Greene and J. G. Venegas, "Spatial heterogeneity of lung perfusion assessed with ¹³N PET as a vascular biomarker in chronic obstructive pulmonary disease", *J. Nuclear Med.* **51** (2010) 57–65; doi:10.2967/jnumed.109.065185.
- [34] J. P. Murgo and N. Westerhof, "Input impedance of the pulmonary arterial system in normal man: effects of respiration and comparison to systemic impedance", *Circ. Res.* **54** (1984) 666–673; doi:10.1161/01.RES.54.6.666.
- [35] M. Panaretou and J. Dermellis, "Assessment of left atrial input impedance in normal subjects and in hypertensive patients", *Eur. J. Heart Fail.* **7** (2005) 63–68; doi:10.1016/j.ejheart.2004.03.019.
- [36] H. Piene, "Pulmonary arterial impedance and right ventricular function", *Phys. Rev.* **66** (1986) 606–652; doi:10.1152/physrev.1986.66.3.606.
- [37] A. Postles, A. R. Clark and M. H. Tawhai, "Dynamic blood flow and wall shear stress in pulmonary hypertensive disease", in: *Proceedings of the 36th Annual International Conference of the IEEE Engineering in Medicine and Biology Society (EMBC)* (Engineering in Medicine and Biology Society (EMBC), 2014) 5671–5674; doi:10.1109/EMBC.2014.6944914.
- [38] A. R. Pries, T. W. Secomb and P. Gaetgens, "Biophysical aspects of blood flow in the microvasculature", *Cardiovasc. Res.* **32** (1996) 654–667; doi:10.1016/S0008-6363(96)00065-X.
- [39] M. Proenca, F. Braun, J. Sola, J.-P. Thiran and M. Lemay, "Noninvasive pulmonary artery pressure monitoring by EIT: a model-based feasibility study", *Med. Biol. Eng. Comput.* **55** (2017) 949–963; doi:10.1007/s1151.
- [40] M. U. Qureshi, G. D. A. Vaughan, C. Sainsbury, M. Johnson, C. S. Peskin and M. S. Olufsen, "Numerical simulation of blood flow and pressure drop in the pulmonary arterial circulation", *Biomech. Model. Mechanobiol.* **13** (2014) 1137–1154; doi:10.1007/s10237-014-0563-y.
- [41] V. K. Sud and G. S. Sekhon, "Arterial flow under periodic body acceleration", *Bull. Math. Biol.* **47** (1985) 35–52; doi:10.1007/BF02459645.
- [42] A. J. Swan, A. R. Clark and M. H. Tawhai, "A computational model of the topographic distribution of ventilation in healthy human lungs", *J. Theor. Biol.* **300** (2012) 222–231; doi:10.1016/j.jtbi.2012.01.042.
- [43] W. Tan, K. Madhavan, K. S. Hunter, D. Park and K. R. Stenmark, "Vascular stiffening in pulmonary hypertension: cause or consequence? *Pulm. Circ.* **4** (2014) 560–580; doi:10.1086/677370.

- [44] M. H. Tawhai, A. R. Clark and K. S. Burrowes, “Computational models of the pulmonary circulation: insights and the move toward clinically directed studies”, *Pulm. Circ.* **1** (2011) 224–238; doi:10.4103/2045-8932.83452.
- [45] J. G. Venegas, T. Winkler, G. Musch, M. F. Vidal Melo, D. Layfield, N. Tgavelekos, A. J. Fischman, R. J. Callahan, G. Bellani and R. S. Harris, “Self-organized patchiness in asthma as a prelude to catastrophic shifts”, *Nature* **434** (2005) 777–782; doi:10.1038/nature03490.
- [46] Z. Wang and N. C. Chesler, “Pulmonary vascular wall stiffness: an important contributor to the increase right ventricular afterload with pulmonary hypertension”, *Pulm. Circ.* **1** (2011) 212–223; doi:10.4103/2045-8932.83453.
- [47] J. B. West, *Respiratory physiology - the essentials* (Williams and Wilkins, Baltimore, MD, 1995).
- [48] J. B. West, C. T. Dollery and A. Naimark, “Distribution of blood flow in isolated lung; relation to vascular and alveolar pressures”, *J. Appl. Phys.* **19** (1964) 713–724; doi:10.1152/jappl.1964.19.4.713.
- [49] F. Wiener, E. Morkin, R. Skalak and A. P. Fishman, “Wave propagation in the pulmonary circulation”, *Circ. Res.* **19** (1966) 834–850; doi:10.1161/01.RES.19.4.834.
- [50] J. R. Womersley, “Oscillatory motion of a viscous liquid in a thin walled elastic tube. I: the linear approximation for long waves”, *Lond. Edinb. Dubl. Phil. Mag. J. Sci.* **46** (1955) 199–221.
- [51] E. B. Wylie and V. Streeter, *Fluid transient* (McGraw-Hill, New York, NY, 1978).
- [52] R. T. Yen, Y. C. Fung and N. Bingham, “Elasticity of small pulmonary arteries in the cat”, *J. Biomech. Eng.* **102** (1980) 170–177; doi:10.1115/1.3138218.
- [53] Q. Zhou, J. Gao, W. Huang and R. T. Yen, “Vascular impedance analysis in human pulmonary circulation”, *Proceedings of IMECE AMSE International Mechanical Engineering Congress and Exposition, IMECE2002–33525* (2002); doi:10.1115/IMECE2002-33525.
- [54] F. Y. Zhuang, Y. C. Fung and R. T. Yen, “Analysis of blood flow in cat’s lung with detailed anatomical and elasticity data”, *J. Appl. Phys.* **55** (1983) 1341–1348; doi:10.1152/jappl.1983.55.4.1341.